Journal of Electronic Materials (2022) 51:6568–6578
https://doi.org/10.1007/s11664-022-09898-9

ORIGINAL RESEARCH ARTICLE

# First-Principles Insight into a $B_4C_3$ Monolayer as a Promising Biosensor for Exhaled Breath Analysis

Uzma Nosheen[1] · Abdul Jalil[1] · Syed Zafar Ilyas[1] · Ahsan Illahi[2] · Sayed Ali Khan[3] · Ather Hassan[1]

Received: 14 June 2022 / Accepted: 19 August 2022 / Published online: 19 September 2022


## Abstract

Nanomaterial-based room temperature gas sensors are used as a screening tool for diagnosing various diseases through breath analysis. The stable planar structure of boron carbide ($B_4C_3$) is utilized as a base material for adsorption of human breath exhaled VOCs, namely formaldehyde, methanol, acetone, toluene along, with interfering gases of carbon dioxide and water. The adsorption energy, charge density, density of states, energy band gap variation, recovery time, sensitivity, and work function of adsorbed molecules on pristine $B_4C_3$ are analyzed by density functional theory. The computed adsorption energies of VOC are in the range of $-0.176$ to $-0.238$ eV, and a larger interaction distance validate the physisorption behavior of these VOCs biomarkers on pristine boron carbide monolayer. Minute changes are determined from the electronic band structure of all adsorbed systems conserving the semiconducting nature of the $B_4C_3$ monolayer. The band gap variation upon adsorption of VOCs and interfering gases is examined between 0.05 and 0.52%. The $13.63 \times 10^{-9}$ s recovery time of methanol is slower among VOCs, and $0.556 \times 10^{-9}$ s of carbon dioxide ($CO_2$) is faster for desorption. The results reveal that boron carbide can be utilized as a biosensor at room temperature for the analysis of exhaled VOCs from human breath.

### Graphical abstract

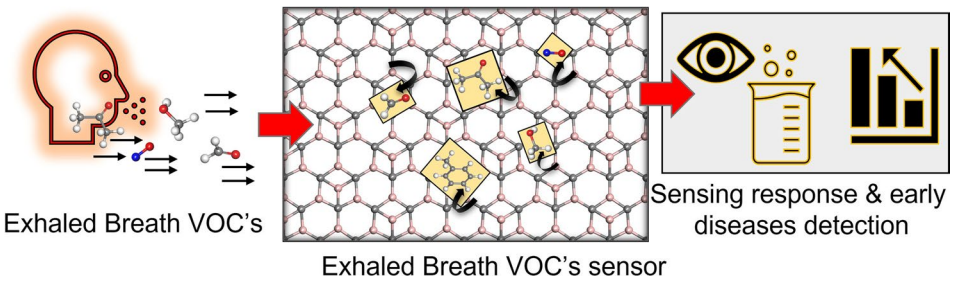


**Keywords** Exhaled breath analysis · B4C3 monolayer · biosensor · DFT study

## Introduction

Following the severe consequences of Covid-19, researchers are pursuing novel methods for early disease detection. Existing capabilities for early disease detection through efficient, simple, low-cost and noninvasive mechanisms are desperately required. Human exhaled breath offers a reasonable, inexpensive, and rapid revealing practice.[1,2] Exhaled breath of human comprises of a mixture of water, carbon dioxide, oxygen, nitrogen and other traces of volatile organic compounds.[3,4] Volatile organic compounds (VOCs) identification has

✉ Abdul Jalil
abdul.jaleel@aiou.edu.pk

1 Department of Physics, Allama Iqbal Open University, Islamabad, Pakistan

2 Research in Modeling and Simulation Group (RIMS), Department of Physics, COMSATS University, Islamabad, Pakistan

3 Department of Chemistry and Chemical, Rutgers, The State University of New Jersey, Jersey, NJ 08854, USA

become an important objective.[5–8] The higher concentration of VOCs in indoor air is detrimental to human health. VOCs having low boiling points and higher vapor pressure, such as methanol, ethanol, formaldehyde, acetone, and ammonia, are the primary causes of indoor air pollution.[9–12] Exhaled human breath can be used to examine these molecules as biomarkers for a variety of disorders, including new coronavirus, liver cirrhosis, diabetes, lung cancer, and tuberculosis.[13–18] Around 870 VOCs carry information about dysfunction in the human body.[3,19] More than 3500 VOCs are identified in parts per million (ppm) or parts per trillion (ppt) concentration as a part of human breathing out.[20] Gas chromatography-mass spectroscopy used in clinical trials can detect VOCs concentration between 1 and 5000 parts per billion (ppb). As a screening tool, this technology requires more time and expensive equipment.[21–24] So enormous efforts are being made to develop simple and efficient sensors for detecting the lower concentration of VOCs at parts per billion.

Purposefully, semiconductor gas sensors[25] are extensively employed for the detection of VOCs with alteration of electronic conductivity after and before gas adsorption.[26–28] To boost the sensitivity of semiconductor-based gas sensors, low dimensionality and easily adjustable features of two-dimensional (2D) materials[29–31] have enchanted intensive research in inorganic[32–35] and organic[36–38] gas identification. 2D materials for example graphene,[39–43] phosphorene,[26,44,45] stanene,[46–48] arsenene,[49] silicone,[50,51] borophene,[52,53] molybdenum disulfide ($MoS_2$),[13,54–60] tungsten disulfide ($WS_2$)[61] monolayers have been investigated for the adsorption of small gas molecules and VOCs as well. Numerous compounds, elemental crystals, and atomically thin materials with exceptional electronic and mechanical properties are formed by lighter elements such as carbon (C), boron (B), and nitrogen (N).[62] Experimentally synthesized a chemically inert material, boron carbide sheets with boron as a dopant possess the same structure as graphene but exorbitantly changed characteristics to utilize in electronic devices.[63–65] Boron carbide ($BC_3$) monolayer serves as a gas sensor for harmful carbonaceous pollutants[66–69] and is highly selective and sensitive to acetone.[70] Another 2D monolayer, $BC_6N$, has been recently examined for human breath analysis[71] and proved to be a potential candidate for ethanol.[19] Among other 2D B-C compounds, a highly stable semiconducting $B_4C_3$ monolayer[62] evolved from a hypothetically designed B4C3 cluster in 2000.[72] The planar structure of B4C3 has been recently investigated as a toxic gas sensor for carbon monoxide (CO), sulfur dioxide (SO2), nitrogen oxide (NO), ammonia (NH3), and hydrogen sulfide (H2S).[73]

Inspired by the thermal and dynamic stability of the B4C3 monolayer,[74] a comprehensive analysis is presented on the adsorption of various volatile organic compounds (VOCs) such as methanol (CH3OH), formaldehyde (H2CO), toluene (C7H8) and acetone (C3H6O) on B4C3 monolayer as familiar breath biomarkers. These molecules belong to aldehydes, ketones, and alcohols of different functional groups of hydrocarbons. Carbon dioxide (CO2) and water (H2O) are used as interfering gases expected to create hindrance in the detection of biomarkers. Density functional theory (DFT) is employed to explore the adsorption capabilities of VOCs. This research aims at early detection of disease by VOCs identification on $B_4C_3$ monolayer. The results explain the superior sensing properties of $B_4C_3$ adsorption energies, charge analysis, band structure, density of states, and recovery time.

## Computational Methods

Based on DFT, Vienna Ab-initio Simulation Package (VASP) is adapted to carry out all calculations. The projector augmented wave method[75] is employed for ion–electron interactions. Perdew-Burke-Ernzerhof with generalized gradient approximation (PBE-GGA),[76,77] is implemented for exchange–correlation potential. Grimme's DFT-D3 correction[78] is being applied for the adsorption properties of VOCs. During geometry optimization, the Brillouin zones are sampled using a $3\times3\times1$ k-point grid Monkhorst–Pack scheme.[30] The plane wave basis is fixed at 500 eV. Using the quasi-Newton approach of Broyden-Fletcher-Goldfarb-Shanno (LBFGS), all of the structures with full relaxation of stress and force on each atom are evaluated to be less than 0.001 eV/Å$^3$ and 0.01 eV/Å, respectively. The supercell size of $2\times2\times1$ is being preserved for $B_4C_3$ monolayer.

For band structure computations, Heyd-Scuseria-Ernzerhof (HSE06) hybrid functional[79] for band is being executed. The interaction between the adsorbent monolayer and adsorbed molecules is quantitatively described by the van der Waals (vdW) corrected adsorption energy and can be expressed as:

$$E_{ads} = E_{total} - E_{monolayer} - E_{molecule} \quad (1)$$

where $E_{ads}$ is the adsorption energy, $E_{total}$ is the combined energy of monolayer and molecule. $E_{monolayer}$ and $E_{molecule}$ are the adsorption energies of an individual monolayer and the isolated molecule. The criteria used to determine the physical adsorption of VOCs on the monolayer is exothermic adsorption ($<0$ eV). $E_{ads}<0.5$ eV is an indicator of physisorption.[80] Stronger gas adsorption is indicated by the larger negative value of $E_{ads}$. Furthermore, the Bader charge method is obtained to analyze the behavior of charge transfer upon molecule adsorption.[81] The charge density difference upon the adsorption of gas molecule is computed by the following expression.

$$\Delta\rho = \rho_{total} - \rho_{monolayer} - \rho_{molecule} \quad (2)$$

whereas $\Delta_\rho$ is the charge density difference. Total charge density of combined system is referred as $\rho_{total}$. The individual charge densities of monolayer and isolated molecule are represented by $\rho_{monolayer}$ and $\rho_{molecule}$.[82]

## Results and Discussion

### *Pristine $B_4C_3$*

The monolayer of $B_4C_3$ is a network of $B_4C_3$ ordered patterns that are arranged to each other structurally. Each $B_4C_3$ unit accompanying a B atom at the center is enclosed by hollow $B_3C_3$ rings, and the entire unit is coupled to the nearby $B_4C_3$ array by B-C bonds, as depicted in Fig. 1a. The central boron atoms of all $B_4C_3$ formations are positioned at ca. 0.3 Å above the hexagonal rings, giving the structure a buckled appearance. Two types of coordination exist in the boron atoms ($B_1$ and $B_2$). One of the B atoms ($B_1$) is placed in the middle of the hexa coordinated ring consisting of three C and three $B_2$ atoms. While the other atom, $B_2$ is positioned at the corner with tetra coordination comprising one $B_1$ and three C atoms. So the structure displays the $B_1$-$B_2$ bond distance as 1.69 Å closer to the $B_4C_3H_6$ cluster (1.77 Å) and 2D borophene (1.70 Å). Due to hyperconjugation and different geometrical positions, three types of B-C bonds appear; the first bond $B_2$-C (1.52 Å) connects the neighboring $B_4C_3$ cluster, and another bond $B_2$-C (1.55 Å) exists at the edge points of $B_3C_3$ ring, third bond $B_1$-C has the bond length of 1.59 Å. These bond lengths are in accordance with the $BC_3$ structure (1.58 Å). Additionally, the B-B bond is consistent with 2D boron. These observations suggest a strong connection between carbon and boron and carbon atoms with tetra coordination bridges $B_4C_3$ cluster. So the planar hyper coordinated (phC) carbon bonds comprising 2D materials exhibit exceptional physiochemical properties.[73,74]

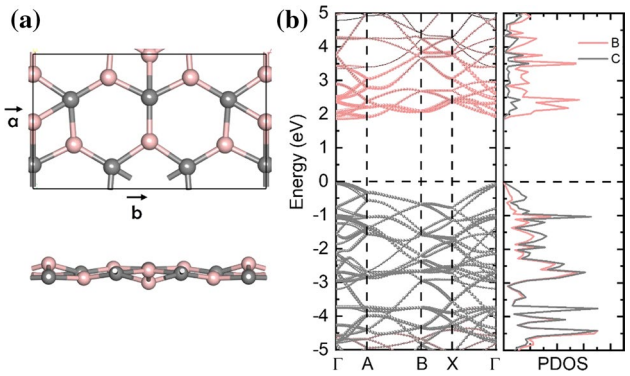


**Fig. 1** (a) The top and side views of B4C3 monolayer. (b) Band structure along with PDOS of pristine B4C3 monolayer. Grey color represents carbon and pink color represents boron (Color figure online).

### *Electronic Band Structure of Pristine $B_4C_3$*

The $B_4C_3$ monolayer is a direct band gap semiconductor with a band gap of 1.915 eV. The band structure and partial density of states (PDOS) of $B_4C_3$ are illustrated in Fig. 1b. The valence band maximum (VBM) and conduction band minimum (CBM) lie at Γ point.[73] Fermi level lies at 0 eV. The electronic configurations of B and C are [He] $2s^2 2p^1$ and [He] $2s^2 2p^2$. It is clear from the electronic configuration that the p orbitals of B and C form conduction and valence bands, which is consistent with PDOS of $B_4C_3$.

This work investigates the adsorption geometries of VOCs, including $C_3H_6O$, $CH_3OH$, $H_2CO$ and $C_7H_8$, along with $CO_2$ and $H_2O$. Each molecule is deposited on the $B_4C_3$ monolayer with a different orientation. Adsorption energies, charge analysis, total density of states, band gap, recovery time of adsorbed gases, and work function are analyzed for each adsorbed system on $B_1$ site and are enlisted in Table I. All the molecules show physisorption. $B_4C_3$ monolayer proves to be a good sensor for all physisorbed molecules.

A supercell of $3 \times 3$ is assumed to study the adsorption of gas molecules on the pristine $B_4C_3$ monolayer, comprising 32 B atoms and 23 C atoms. Each gas molecule prefers a specific molecular orientation. The alignment of molecules can be in a parallel or perpendicular direction with respect to $B_4C_3$ sheet.

**Table I** Absorption energy ($E_{ads}$) in eV, band gap ($E_g$) in eV and charge transfer of adsorbed molecules on $B_4C_3$ (Q) and recovery time (τ) in sec and work function (Φ) in eV

| System | $E_{ads}$ (eV) | $E_g$ (eV) | Q (e) | Recovery time τ ($10^{-9}$ s) | Work function Φ (eV) | Nature of molecule |
|---|---|---|---|---|---|---|
| Pristine $B_4C_3$ | – | 1.915 | – | – | 4.961 | – |
| $H_2CO$-$B_4C_3$ | −0.194 | 1.916 | −0.023 | 2.345 | 4.946 | Acceptor |
| $CH_3OH$-$B_4C_3$ | −0.238 | 1.913 | −0.021 | 13.630 | 4.95 | Acceptor |
| $C_3H_6O$-$B_4C_3$ | −0.176 | 1.917 | −0.004 | 1.141 | 4.885 | Acceptor |
| $C_7H_8$-$B_4C_3$ | −0.21 | 1.914 | −0.005 | 4.447 | 4.806 | Acceptor |
| $CO_2$-$B_4C_3$ | −0.158 | 1.913 | −0.015 | 0.556 | 4.769 | Acceptor |
| $H_2O$-$B_4C_3$ | −0.196 | 1.925 | −0.013 | 2.540 | 5.071 | Acceptor |

### *VOCs Adsorption on $B_4C_3$ Monolayer*

The most stable adsorption geometries of all adsorbed structures are being studied and illustrated in Fig. 2. Formaldehyde has a planar structure with one O atom and two H atoms connected by a central C atom[83].Figure 2a displays an optimized structure of $H_2CO$ on the $B_4C_3$ monolayer taking a parallel tilted orientation of molecule with O atom away from the monolayer and H atoms facing towards the monolayer.

The preferable position of $CH_3OH$ molecule on the $B_4C_3$ surface is parallel but with a tilted axis. The H of the OH group is facing towards the monolayer while methyl group ($CH_3$) is away from the surface, as presented in the top and side view of optimized structure in Fig. 2b. $C_3H_6O$ molecule in Fig. 2c is oriented perpendicularly but tilted in such a way that one atom of H of the methyl ($CH_3$) group gets closer to the C of $B_4C_3$ substrate, and the other $CH_3$ group is away from the substrate. The carbonyl (C = O) group is at a distance to $B_2$ atom and is not parallel to the surface. $C_7H_8$ prefers to adsorb in a perpendicular position with carbon hexagon skewed towards the right and away from $B_4C_3$ monolayer and H of $CH_3$ being closer towards the surface as depicted in Fig. 2d.The position of $CO_2$ molecule is parallel to the $B_4C_3$ surface (Fig. 2e). However, one of the O atoms is slightly tilted towards the surface. $H_2O$ prefers to adsorb on the $B_4C_3$ monolayer in the parallel orientation. O atom is pointing the monolayer surface outwards with the H atom facing toward the surface, as illustrated by the optimized structure in Fig. 2f.

For the development of efficient gas sensors, strong as well as weak interactions between the gas molecule and the substrate must exist. The strong interaction is required to retain the gas molecule on the substrate surface, and weak interaction is necessary for removing of gas molecules from the substrate without damaging the substrate's properties.[19,54]

Adsorption energy provides information about the strength/extent of interaction between the sensing substrate and the adsorbed gas molecule. The $E_{ads}$ values of adsorption of gas molecules shLi et al., 2021ould be between − 0.40 eV (strong physisorption) to − 1.00 eV (weak chemisorption) for an efficient sensing mechanism.[69] A direct relationship exists between the adsorption energy and the sensitivity of the material. A larger value of adsorption energy leads to stronger interaction between the monolayer and gas molecules, which will enhance the sensitivity of the material. On the other hand, strong interaction makes desorption of gas molecules difficult from the material for a reusable gas sensors.[84–86]

The adsorption energies of $H_2CO$, $CH_3OH$, $C_3H_6O$, $C_7H_8$, $CO_2$ and $H_2O$ are computed to be − 0.194 eV, − 0.238 eV, − 0.176 eV, − 0.21 eV, − 0.158 eV and − 0.196 eV. These values confirm weak physical adsorption of all gas molecules onto the pristine $B_4C_3$ monolayer. These adsorption energies are lower than those reported for $H_2CO$ (− 0.228 eV), $CH_3OH$ (− 0.316), $C_3H_6O$ (− 0.381 eV), $C_7H_8$ (− 0.910 eV),

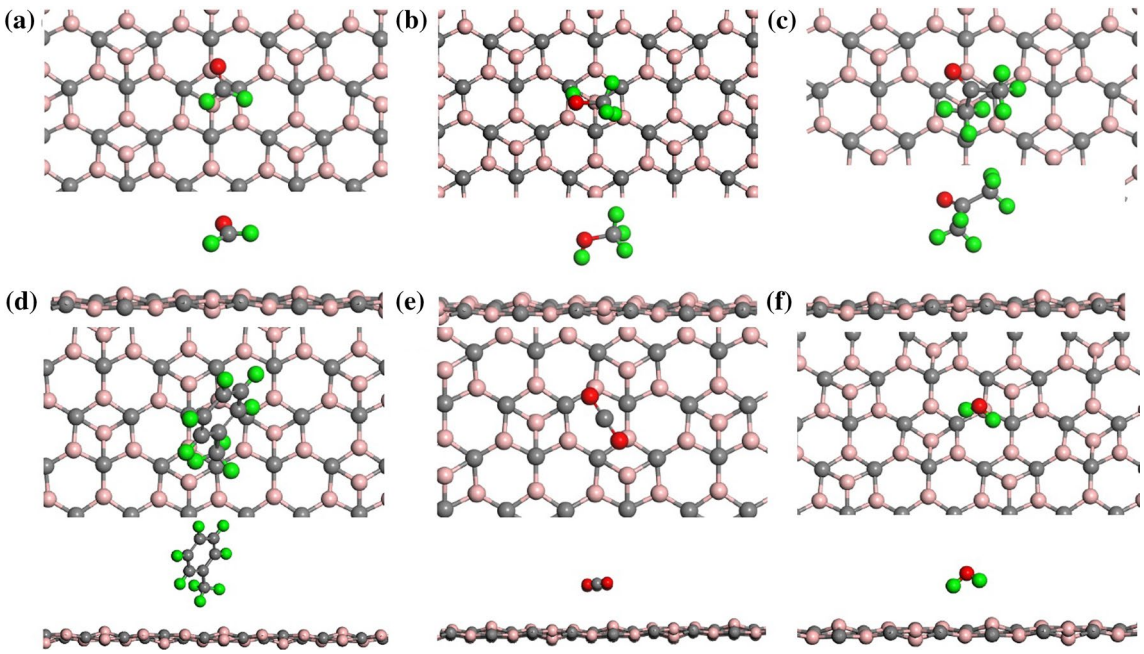


**Fig. 2** The optimized structures (top and side view) of (a) formaldehyde, (b) methanol, (c) acetone, (d) toluene, (e) carbon dioxide and (f) water molecules on pristine $B_4C_3$ monolayer. Grey, pink, green, and red colors represent Carbon, Boron, Hydrogen and Oxygen (Color figure online).

$CO_2$ (−0.253 eV) and $H_2O$ (0.263 eV) on pristine $BC_6N$ nanosheet.[19] The values of adsorption energies of $C_3H_6O$ (−0.320 eV) and $C_7H_8$ (−0.432 eV) on black phosphorus[84] are also greater than calculated pristine $B_4C_3$. The interaction of $H_2CO$ (−0.091 eV) ,[87] $CO_2$ (−0.03 eV), and $H_2O$ (0.05 eV)[88] on graphene are found to be weaker than those accomplished for pristine $B_4C_3$ monolayer. The adsorption energy of $H_2CO$ is −0.556 eV on pristine carbon nitride ($C_2N$) monolayer.[89] The estimated adsorption energy values (i.e., −0.18 eV, −0.33 eV, −0.40 eV, and −0.60 eV) demonstrate subsistent interaction of $H_2CO$, $CH_3OH$, $C_3H_6O$, and $C_7H_8$ on pristine oxygen-terminated titanium carbide MXenes ($Ti_2CO_2$).[90] Adsorption of alcohol molecules on germanene[91] and stanene[92] nanosheets is prominent and occurs due to the presence of the OH group. In this scenario, the reported values of adsorption energy are −1.76 eV for $H_2CO$, −1.95 eV and −1.65 eV for $CH_3OH$. The adsorption energies of $CH_3OH$ (−0.47 eV), $C_3H_6O$ (−0.69 eV), and $C_7H_8$ (−1 eV) on oxidized molybdenum carbide MXene ($Mo_2CO_2$)[93] are greater than $B_4C_3$. It shows that $B_4C_3$ monolayer performs better than pristine graphene but is less sensitive than other 2D materials.

The small value of adsorption energy and the large value of the distance between the molecule and the substrate reveal physical adsorption due to weak van der Waals interaction.[94–96]

After adsorption of gas molecules, $B_1$-C bond length slightly shortens up to 1.57 Å from 1.59 Å and $B_2$-C bond lengths slightly increase from 1.52 Å to 1.53 Å, and from 1.55 Å to 1.58 Å. The interaction distance between all the gas molecules and $B_4C_3$ monolayer is computed to be greater than 3 Å exhibiting weak physisorption of gas molecules.

## Charge Density Analysis

Due to physisorption, gas molecules and monolayers exchange a minute amount of charge.[19] The charge transfer is computed in terms of Bader charge analysis in order to understand the adsorption better. The Bader charge (Q) analysis determines whether the base material functions as a donor or acceptor. The charge transfer calculated between $B_4C_3$ monolayer and $H_2CO$, $CH_3OH$, $C_3H_6O$, $C_7H_8$, $CO_2$ and $H_2O$ is −0.023 e, −0.021 e, −0.004 e, −0.005 e, −0.015 e, and −0.013 e, respectively.

The differential charge density for all six adsorbed molecules is also depicted in Fig. 3a, b, c, d, e and f. From Fig. 3, it is confirmed that all molecules acquire charge from $B_4C_3$ monolayer upon adsorption, acting as electron acceptors.

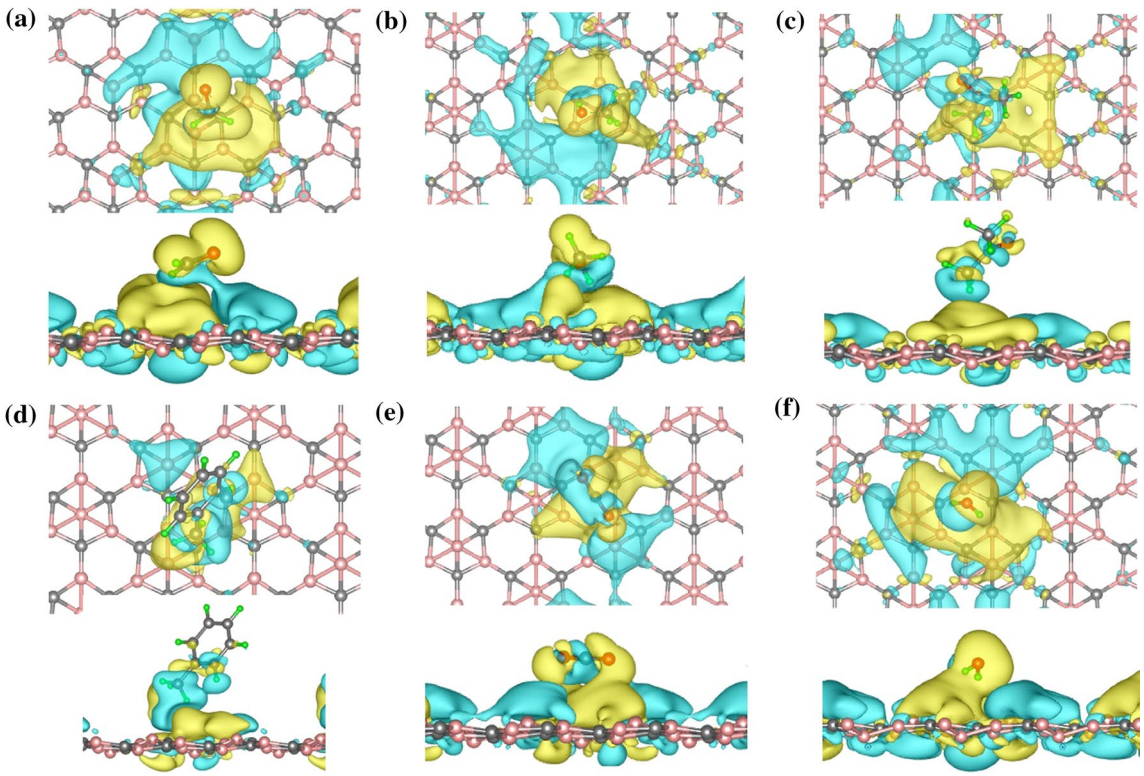


**Fig. 3** Differential charge density (top and side view) of (a) formaldehyde, (b) methanol, (c) acetone, (d) toluene, (e) carbon dioxide and (f) water molecules on pristine $B_4C_3$ monolayer. Cyan and yellow colors shows the charge depletion and accumulation. Colors represent Carbon (grey), Boron (pink), Hydrogen (green) and Oxygen (red) (Color figure online).

The cyan color shows the depletion of charge, and the yellow color depicts the accumulation of charge. B transfers electrons to C of $B_4C_3$ framework indicating the chemical bonding between them. There also exists an ionic bonding in the framework. The cyan color in $B_4C_3$ framework shows the substrate is losing charge near the region of interaction, and the yellow color around the molecule indicates charge accumulation. O, the most electronegative atom, gains more charge from the molecule and the substrate in O containing molecules. In $C_7H_8$, C, with the electronegativity of 2.5, has greater power to attract electrons as compared to B (2.04) and H (2.20). $B_4C_3$ is an electron donor.

## Density of States and Band Structure Analysis

Adsorption of molecules changes the electronic properties of the sensor.[19,97] For this purpose, the electronic band structure and partial density of states (PDOS) of pristine and gas molecules adsorbed on $B_4C_3$ monolayer are displayed in Fig. 4. The energy band gap of pristine $B_4C_3$ is computed as 1.915 eV. Slight change in band structure is observed in the presence of $H_2CO$, $CH_3OH$, $C_3H_6O$, $C_7H_8$, $CO_2$ and $H_2O$ with band gaps of 1.916 eV, 1.913 eV, 1.917 eV, 1.914 eV, 1.913 eV, and 1.925 eV. These values are in close proximity with the small adsorption energy values of adsorbed systems.

In Fig. 4, the Fermi level is represented by 0 eV, and the density of states spans from − 5 to 5 eV. $B_2$-p orbitals and C-p orbitals contribute to the VBM and CBM.[74] Above 0 eV, the peaks of p states of B are more pronounced in the conduction band. The contribution of O-p states (red color) are seen below the Fermi level in the case of $H_2CO$, $CH_3OH$, $C_3H_6O$, $CO_2$ and $H_2O$ (Fig. 4b, c, d, e, f and g).The p orbital of C and s orbital of H of $CH_3$ interact with the hybridized orbitals of $B_4C_3$. The contribution of H states can be seen above 3 eV (above Fermi level) and below − 3 eV in the density of states (DOS) as depicted in Fig. 4e.

It shows that the adsorbed molecules have a minor impact on the electronic properties of pristine $B_4C_3$ monolayer. Although the adsorbed molecules contribute to the conduction and valence bands of pristine monolayer, they make no significant changes to the electronic characteristics of pristine $B_4C_3$ monolayer. The monolayer show semiconducting behavior after weak physisorption of molecules.[19] Owing to larger distance and physical adsorption of molecules, orbital

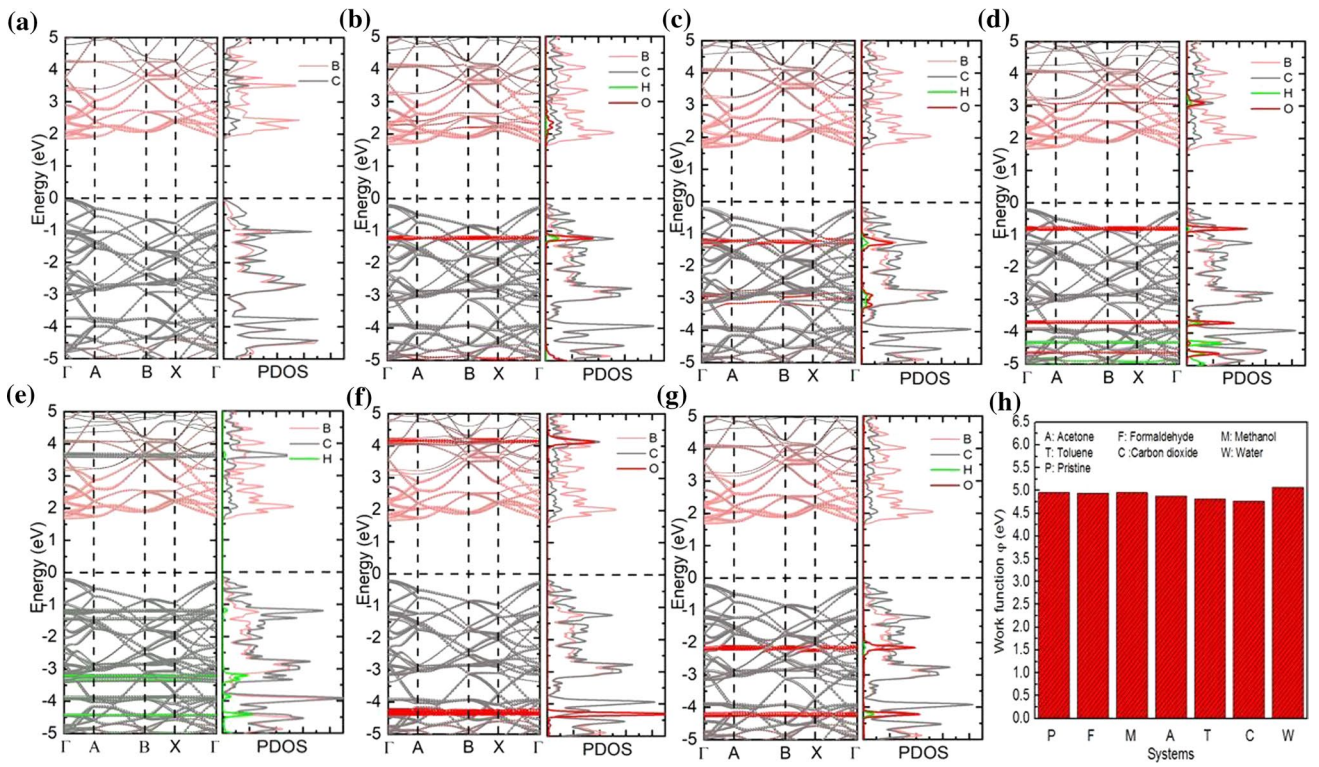


**Fig. 4** Energy band structures and density of states of (a) pristine $B_4C_3$ monolayer, (b) formaldehyde, (c) methanol, (d) acetone, (e) toluene, (f) Carbon dioxide and (g) water molecules on pristine $B_4C_3$ monolayer. The dashed line indicates the Fermi level. Grey (carbon), Pink (boron), Green (hydrogen) and Red (oxygen), (h) Comparison of work function of pristine and adsorbed gas molecules on $B_4C_3$ monolayer, P: Pristine $B_4C_3$ monolayer, F: formaldehyde, M: methanol, A: acetone, T: toluene, C: carbon dioxide and W: water pristine $B_4C_3$ monolayer (Color figure online).

hybridization favors charge transfer between monolayer and gas molecules.[98]

In summary, generally, more adsorption energy and a greater amount of charge transfer enhance the sensitivity of a sensor. The physical adsorption perturbs the electronic states of the gas molecule and the sensor to a minimum level.[99] Theoretically, sensing involves orbital interaction and charge transfer. However, from a practical perspective, more negative adsorption energy is not beneficial since it will be difficult to desorb the biomolecule for subsequent usage of the sensor.[100]

### *Sensing Explanation of the $B_4C_3$ Monolayer*

The energy band gap variation for all absorbed molecules is calculated from the following expression[49];

$$E_g^a\% = \left(\frac{E_{g(pristine)} - E_{g(adsorbed)}}{E_{g(pristine)}}\right) \times 100 \quad (3)$$

where $E_g^a$ is the average band gap energy, $E_{g(pristine)}$ and $E_{g(adsorbed)}$ represent band gap energies of pristine and adsorbed $B_4C_3$ systems. The adsorption of $H_2CO$, $CH_3OH$, $C_3H_6O$, $C_7H_8$, $CO_2$ and $H_2O$ slightly alter the band gap energy. The energy band gap variation for $CH_3OH$, $C_3H_6O$ and $CO_2$ is noticed as 0.10% and 0.05% for $H_2CO$ and $C_7H_8$, while for $H_2O$, it is 0.52%. The variation supports the physisorption behavior of adsorbed molecules. Alteration in band gap results in the conductivity of the system, which is negligible in this case. The pristine $B_4C_3$ monolayer distinguishes the specific type of VOC based on the sensitivity. Sensitivity of the monolayer can be estimated by adsorption energy, charge transfer and band gap.[19,101] The $B_4C_3$ monolayer shows moderate sensitivity towards methanol. Moreover, surface functionalization[13,102] of monolayer and introduction of molecular sieve[103] will be utilized to avoid the interference between target VOCs and interfering gases.

For a reusable gas sensor, the gas molecules are capable enough to desorb themselves from the sensing material after detection.[31] So the performance of a gas sensor can be evaluated by its recovery time ($\tau$).[104] Using transition state theory, $\tau$ can be expressed as;

$$\tau = \nu_o^{-1} e^{(-E_{ads}/kT)} \quad (4)$$

In the above expression, $\nu_o$ ($10^{12}$ Hz) is the attempt frequency for visible light, k is Boltzmann constant, T is the room temperature at 300 K, and $E_{ads}$ is the adsorption energy of adsorbed systems. From this equation, a longer recovery time is expected for a large (more negative) value of $E_{ads}$, which will slow down the desorption process of gas molecules.[19] The recovery time for all molecules is listed in Table I. The calculated recovery time for $H_2CO$, $CH_3OH$, $C_3H_6O$, $C_7H_8$, $CO_2$ and $H_2O$ are $2.345\times10^{-9}$ s, $13.630\times10^{-9}$ s, $1.141\times10^{-9}$ s, $4.447\times10^{-9}$ s, $0.556\times10^{-9}$ s and $2.540\times10^{-9}$ s. It shows that the $CH_3OH$ ($\tau = 13.630\times10^{-9}$ s) and $CO_2$ ($\tau = 0.556\times10^{-9}$ s) possess the highest and lowest recovery time at a constant temperature. The Desorption process of $CH_3OH$ is slower, while the Desorption of $CO_2$ is faster than other molecules. The reversibility of the sensor can be better achieved as the VOCs are physically adsorbed on the $B_4C_3$ monolayer with ease of desorption process.[18,98]

### Work Function

The electrical conductivity of a system is related to its work function alteration.[69] The adsorption of gases on the sensing material creates surface charge redistribution, which will alter the material's work function ($\Phi$). The energy required to remove an electron from Fermi level to infinity is known as the work function. It is calculated by the following expression;

$$\Phi = V(\Phi) - E_f \quad (5)$$

Here, V ($\Phi$) represents the electrostatic potential at the vacuum level, and $E_f$ denotes the potential at the Fermi energy level. $\Phi$ is sensitive to any change that occur at the surface due to gas adsorption.[105] The transmission of charge between the sensing material and gas molecules establishes a dipole moment in the physisorption process. There will be a variation in the work function, which may lead to more changes in the sensing properties of an adsorbed system. The values of work function are summarized in the Table I. The work function for pristine $B_4C_3$ monolayer is 4.961 eV. The adsorbed gas molecules of $H_2CO$, $CH_3OH$, $C_3H_6O$, $C_7H_8$ and $CO_2$ show a minor decreasing trend from 4.95 eV to 4.769 eV as displayed in Fig. 4h. The work function for $H_2O$ adsorbed system is computed to be 5.071 eV, slightly greater than 4.961 eV of pristine $B_4C_3$. The greater value of work function of $H_2O$ from pristine $B_4C_3$ monolayer means the electron overflow from Fermi to vacuum level in pristine monolayer is obstructed by $H_2O$ adsorption. However the reduction in work function exhibits greater electron mobility.[106] The results reveal an almost negligible change in the work function of all systems compared to pristine monolayer. This indicates a very weak physisorption of all gas molecules. Nevertheless the change in work function shows that $B_4C_3$ monolayer is favorable for gas sensing.

## Conclusion

Gleaned from the framework of DFT, this proposed study computes the structural and electronic properties of human breath exhaled VOCs adsorbed onto boron carbide

monolayer. The adsorption energies, charge analysis and band structure, recovery time, and work function of VOCs, including formaldehyde, methanol, acetone, Toluene and interfering gases of $CO_2$ and $H_2O$ are being studied. When VOCs adsorb on $B_1$ site of pristine $B_4C_3$ monolayer, their adsorption energies fall in between 0.158 eV and 0.238 eV. The results reveal physisorption nature of all molecules. Among all other molecules, methanol shows the highest adsorption energy. O functionalized VOCs display less adsorption energies. Due to very weak physisorption and large interaction distance between molecules and monolayer, less charge has transferred from boron carbide monolayer to adsorbed molecules. So, VOCs along with $CO_2$ and $H_2O$ are exposed to be charge acceptors. The band gap of the adsorbed systems does not change and lies in the range of 1.913–1.925 eV. Less apparent changes are discovered (0.05% to 0.52%) in the electronic properties of boron carbide layer after the interaction with VOCs. The calculated work function for $H_2O$ is greater (5.071 eV) and lower for $CO_2$ (4.769 eV) compared to pristine $B_4C_3$. The recovery time for $CO_2$ is greater than all other considered molecules. The results conclude that pristine $B_4C_3$ monolayer can be used as a potential candidate for sensing VOCs for breath analysis.

## Declarations

**Conflict of interest** The authors declare no conflict of interest.

## References


1. Q.A. Drmosh, I. Olanrewaju Alade, M. Qamar, and S. Akbar, Zinc Oxide-based Acetone Gas Sensors for Breath Analysis: a Review. *Chem. - An Asian J.* 16, 1519 (2021).
2. A.T. Güntner, N.J. Pineau, D. Chie, F. Krumeich, and S.E. Pratsinis, Selective Sensing of Isoprene by Ti-Doped ZnO for Breath Diagnostics. *J. Mater. Chem. B* 4, 5358 (2016).
3. B. De Lacy Costello, A. Amann, H. Al-Kateb, C. Flynn, W. Filipiak, T. Khalid, D. Osborne, and N.M. Ratcliffe, A Review of the Volatiles from the Healthy Human Body. *J. Breath Res.* 8, 014001 (2014).
4. J. Rudnicka, T. Kowalkowski, and B. Buszewski, Searching for Selected Vocs in Human Breath Samples as Potential Markers of Lung Cancer. *Lung Cancer* 135, 123 (2019).
5. H. Chen et al., NiO–ZnO Nanoheterojunction Networks for Room-Temperature Volatile Organic Compounds Sensing. *Adv. Opt. Mater.* 6, 1 (2018).
6. V. Postica et al., Tuning ZnO Sensors Reactivity Toward Volatile Organic Compounds Via AG Doping and Nanoparticle Functionalization. *ACS Appl. Mater. Interfaces* 11, 31452 (2019).
7. X. Chen, R. Behboodian, D. Bagnall, M. Taheri, and N. Nasiri, Metal-Organic-Frameworks: Low Temperature Gas Sensing and Air Quality Monitoring. *Chemosensors* 9, 1 (2021).
8. Y. Zhao et al., Construction of Zn/Ni Bimetallic Organic Framework Derived ZnO/NiO Heterostructure with Superior n-Propanol Sensing Performance. *ACS Appl. Mater. Interf* 13, 9206 (2021).
9. K. Toda, R. Furue, and S. Hayami, Recent Progress in Applications of Graphene Oxide for Gas Sensing: a Review. *Anal. Chim. Acta* 878, 43 (2015).
10. H. Guo, S.C. Lee, L.Y. Chan, and W.M. Li, Risk Assessment of Exposure to Volatile Organic Compounds in Different Indoor Environments. *Environ. Res.* 94, 57 (2004).
11. T. Salthammer, Very Volatile Organic Compounds: an Understudied Class of Indoor Air Pollutants. *Indoor Air* 26, 25 (2016).
12. S. Wang, H.M. Ang, and M.O. Tade, Volatile Organic Compounds in Indoor Environment and Photocatalytic Oxidation: State of the Art. *Environ. Int.* 33, 694 (2007).
13. W.Y. Chen, C.C. Yen, S. Xue, H. Wang, and L.A. Stanciu, Surface Functionalization of Layered Molybdenum Disulfide for the Selective Detection of Volatile Organic Compounds at Room Temperature. *ACS Appl. Mater. Interf.* 11, 34135 (2019).
14. X. Li, L. Zhang, Z. Yang, P. Wang, Y. Yan, and J. Ran, Adsorption Materials for Volatile Organic Compounds (VOCs) and the Key Factors for Vocs Adsorption Process: a Review. *Sep. Purif. Technol.* 235, 116213 (2020).
15. T. Lin, X. Lv, Z. Hu, A. Xu, and C. Feng, semiconductor Metal Oxides as Chemoresistive Sensors for Detecting Volatile Organic Compounds. *Sensors* 19, 233 (2019).
16. F. Temel, and S. Kutluay, Investigation of high-Performance Adsorption for Benzene and Toluene Vapors by Calix[4] Arene Based Organosilica (CBOS). *New J. Chem.* 44, 12949 (2020).
17. P. Gouma, A. Prasad, and S. Stanacevic, A Selective Nanosensor Device for Exhaled Breath Analysis. *J. Breath Res.* 5, 1 (2011).
18. U. Srimathi, V. Nagarajan, and R. Chandiramouli, Germanane Nanosheet as a Novel Biosensor for Liver Cirrhosis Based on Adsorption of Biomarker Volatiles – a DFT Study. *Appl. Surf. Sci.* 475, 990 (2019).
19. S.M. Aghaei, A. Aasi, S. Farhangdoust, and B. Panchapakesan, Graphene-Like BC6N Nanosheets are Potential Candidates for Detection of Volatile Organic Compounds (VOCs) in Human Breath: A DFT Study. *Appl. Surf. Sci.* 536, 147756 (2021).
20. A. Rydosz, Sensors for Enhanced Detection of Acetone as a Potential Tool for Noninvasive Diabetes Monitoring. *Sensors (Switzerland)* 18, 1 (2018).
21. D.W. Potter, and J. Pawliszyn, Detection of Substituted Benzenes in Water at the Pg/Ml Level Using Solid-phase Microextraction and Gas Chromatography-Ion Trap Mass Spectrometry. *J. Chromatogr. A* 625, 247 (1992). https://doi.org/10.1016/0021-9673(92)85209-C.
22. T. Miyake, and T. Shibamoto, Quantitative Analysis by Gas Chromatography of Vola tile Carbonyl Compounds in Cigarette Smoke. *J. Chromatogr. A* 693, 376 (1995).
23. S.E. Ebeler, A.J. Clifford, and T. Shibamoto, Quantitative Analysis by Gas Chromatography of Volatile Carbonyl Compounds in Expired Air from Mice and Human. *J. Chromatogr. B Biomed. Appl.* 702, 211 (1997).
24. S. Sethi, R. Nanda, and T. Chakraborty, Clinical Application of Volatile Organic Compound Analysis for Detecting Infectious Diseases. *Clin. Microbiol. Rev.* 26, 462 (2013).
25. A.P. Dral, and J.E. ten Elshof, 2D Metal Oxide Nanoflakes for Sensing Applications: Review and Perspective, Sensors Actuators. *B Chem.* 272, 369 (2018).
26. S. Sun, T. Hussain, W. Zhang, and A. Karton, Blue Phosphorene Monolayers as Potential Nano Sensors for Volatile Organic Compounds under Point Defects. *Appl. Surf. Sci.* 486, 52 (2019).
27. C.R. Minitha, V.S. Anithaa, V. Subramaniam, and R.T. Rajendra Kumar, Impact of Oxygen Functional Groups on Reduced Graphene Oxide-based Sensors for Ammonia and Toluene Detection at Room Temperature. *ACS Omega* 3, 4105 (2018).

28. A. Mirzaei, S.G. Leonardi, and G. Neri, Detection of Hazardous Volatile Organic Compounds (VOCs) by Metal Oxide Nanostructures-based Gas Sensors: a Review. *Ceram. Int.* 42, 15119 (2016).
29. D. Tyagi, H. Wang, W. Huang, L. Hu, Y. Tang, Z. Guo, Z. Ouyang, and H. Zhang, Recent Advances in Two-dimensional-Material-based Sensing Technology Toward Health and Environmental Monitoring Applications. *Nanoscale* 12, 3535 (2020).
30. H.J. M, and J.D. Pack, Special Points for Brillouin-zone Integrations. *Phys. Rev. B* 13, 5188–5192 (1976). https://doi.org/10.1103/PhysRevB.13.5188.
31. X. Tang, A. Du, and L. Kou, Gas Sensing and Capturing Based on two-Dimensional Layered Materials: Overview from Theoretical Perspective. *Wiley Interdiscip. Rev. Comput. Mol. Sci.* 8, 1 (2018).
32. Z. Gao, Y. Sun, M. Li, W. Yang, and X. Ding, Adsorption Sensitivity of fe Decorated Different Graphene Supports Toward Toxic Gas Molecules (CO and NO). *Appl. Surf. Sci.* 456, 351 (2018).
33. H. Tang, L.N. Sacco, S. Vollebregt, H. Ye, X. Fan, and G. Zhang, Recent Advances in 2D/Nanostructured Metal Sulfide-based Gas Sensors: Mechanisms, Applications, and Perspectives. *J. Mater. Chem. A* 8, 24943 (2020).
34. Z.W. Hao, M.M. Dong, R.Q. Zhang, C.K. Wang, and X.X. Fu, An Ultra-sensitive Gas Sensor based on a Two-dimensional Manganese Porphyrin Monolayer. *Phys. Chem. Chem. Phys.* 23, 11852 (2021).
35. S.M. Aghaei, M.M. Monshi, and I. Calizo, A Theoretical Study of Gas Adsorption on Silicene Nanoribbons and its Application in a Highly Sensitive Molecule Sensor. *RSC Adv.* 6, 94417 (2016).
36. A. Aasi, S.M. Aghaei, and B. Panchapakesan, Pt-Decorated Phosphorene as a Propitious Room Temperature VOC Gas Sensor for Sensitive and Selective Detection of Alcohols. *J. Mater. Chem. C* 9, 9242 (2021).
37. F.K. Perkins, A.L. Friedman, E. Cobas, P.M. Campbell, G.G. Jernigan, and B.T. Jonker, Chemical Vapor Sensing with Monolayer MoS2. *Nano Lett.* 13, 668 (2013).
38. V. Nagarajan, and R. Chandiramouli, Novel Method to Detect the Lung Cancer Biomarker Volatiles using Hydrogen Vacant Silicane Nanosheets: A DFT Investigation. *Comput. Theor. Chem.* 1138, 107 (2018).
39. J. Mawwa, S.U.D. Shamim, S. Khanom, M.K. Hossain, and F. Ahmed, In-Plane Graphene/boron Nitride Heterostructures and their Potential Application as Toxic Gas Sensors. *RSC Adv.* 11, 32810 (2021).
40. L. Yang, W. Xiao, J. Wang, X. Li, and L. Wang, Formaldehyde Gas Sensing Properties of Transition Metal-doped Graphene: a First-principles Study. *J. Mater. Sci.* 56, 12256 (2021).
41. K.A.L. Lima, M.L. Pereira Júnior, F.F. Monteiro, L.F. Roncaratti, and L.A. Ribeiro Júnior, $O_2$ Adsorption on Defective Penta-graphene Lattices: a DFT Study. *Chem. Phys. Lett.* 763, 137 (2021).
42. M. Singla, and N. Jaggi, Synergistic Effect of Cu Decoration and N Doping in Divacancy Defected Graphene Nanoribbons on Hydrogen Gas Sensing Properties: DFT Study. *Mater. Chem. Phys.* 273, 125093 (2021).
43. Z. Liang, K. Li, Z. Wang, Y. Bu, and J. Zhang, Adsorption and Reaction Mechanisms of Single and Double $H_2O$ Molecules on Graphene Surfaces with Defects: a Density Functional Theory Study. *Phys. Chem. Chem. Phys.* 23, 19071 (2021).
44. E. Mansouri, J. Karamdel, M. Berahman, and M.T. Ahmadi, Phosphorene as $H_2S$ and $CH_4$ Gas Sensor. *Phys. Status Solidi Appl. Mater. Sci.* 216, 1 (2019).
45. B. Zhang, Z. Mao, and P. Wu, Gas Sensing of Fibrous Red Phosphorene Towards Inorganic Air Pollutants: Insights from First-principles Calculations. *Appl. Surf. Sci.* 565, 150546 (2021).
46. A. Abbasi, and J.J. Sardroodi, Exploration of Sensing of Nitrogen Dioxide and Ozone Molecules using Novel $TiO_2$/Stanene Heterostructures Employing DFT Calculations. *Appl. Surf. Sci.* 442, 368 (2018).
47. Y.Z. Chang, J.N. Lin, S.D. Li, and H. Liu, Adsorption of Greenhouse Gases (Methane and Carbon Dioxide) on the Pure and Pd-adsorbed Stanene Nanosheets: a Theoretical Study. *Surfaces and Interfaces* 22, 100878 (2021).
48. A. Zhang, H. Yang, Q. Liu, W. Li, and Y. Wang, DFT Insights Into the Adsorption Properties of Toxic Gas Molecules on Pure and Transition Metal Embedded Stanene Monolayers: Towards Gas Sensor Devices. *Synth. Met.* 266, 116441 (2020).
49. V. Nagarajan, S. Sundar, and R. Chandiramouli, Interaction studies of Tuberculosis Biomarker Vapours on Novel Beta Arsenene Sheets – a DFT Insight. *Comput. Theor. Chem.* 1205, 113426 (2021).
50. G.K. Walia, D.K.K. Randhawa, and K.S. Malhi, Rise of Silicene and Its Applications in Gas Sensing. *J. Mol. Model.* 27, 107 (2021).
51. G.K. Walia, and D.K.K. Randhawa, First-Principles Investigation on Defect-induced Silicene Nanoribbons — a Superior Media for Sensing $NH_3NO_2$ and NO Gas Molecules. *Surf. Sci.* 670, 33 (2018).
52. M. Ou, X. Wang, L. Yu, C. Liu, W. Tao, X. Ji, and L. Mei, The Emergence and Evolution of Borophene. *Adv. Sci.* 8, 1 (2021).
53. C. Hou, G. Tai, Y. Liu, and X. Liu, Borophene Gas Sensor. *Nano Res.* 15, 2537 (2022).
54. T. Jiang, Q. He, M. Bi, X. Chen, H. Sun, and L. Tao, First-principles Calculations of Adsorption Sensitivity of Au-Doped $MoS_2$ Gas Sensor to Main Characteristic Gases in Oil. *J. Mater. Sci.* 56, 13673 (2021).
55. B. Li, Q. Zhou, R. Peng, Y. Liao, and W. Zeng, Adsorption of SF6 Decomposition Gases ($H_2S$, $SO_2$, $SOF_2$ and $SO_2F_2$) on Sc-Doped $MoS_2$ Surface: a DFT Study. *Appl. Surf. Sci.* 549, 146 (2021).
56. S. Yang, Y. Liu, G. Lei, Y. Xie, L. Peng, H. Xu, Z. Wang, and H. Gu, A DFT Study on the Hydrogen Storage Performance of $MoS_2$ Monolayers Doped with Group 8B Transition Metals. *Int. J. Hydrogen Energy* 46, 24233 (2021).
57. R. Kumar, W. Zheng, X. Liu, J. Zhang, and M. Kumar, $MoS_2$-Based Nanomaterials for Room-Temperature Gas Sensors. *Adv. Mater. Technol.* 5, 1 (2020).
58. A. Shokri, and N. Salami, Gas Sensor Based on $MoS_2$ Monolayer, Sensors Actuators. *B Chem.* 236, 378 (2016).
59. P.X. Zhao, Y. Tang, J. Mao, Y.X. Chen, H. Song, J.W. Wang, Y. Song, Y.Q. Liang, and X.M. Zhang, One-Dimensional $MoS_2$-Decorated $TiO_2$ Nanotube Gas Sensors for Efficient Alcohol Sensing. *J. Alloys Compd.* 674, 252 (2016).
60. N. Baildya, N.N. Ghosh, and A.P. Chattopadhyay, Environmentally Hazardous Gas Sensing Ability of $MoS_2$-Nanotubes: an Insight from the Electronic Structure and Transport Properties. *Nanoscale Adv.* 3, 4528 (2021).
61. C.A. Celaya, M. Boujnah, M. Reina, J. Muñiz, and L.E. Sansores, Theoretical Study of $Au_{20}/WS_2$ Composite Material as a Potential Candidate for the Capture of XO (X=C, N, S) Gases. *Comput. Condens. Matter* 28, e00580 (2021).
62. X. Tian, X. Xuan, M. Yu, Y. Mu, H.G. Lu, Z. Zhang, and S.D. Li, Predicting Two-Dimensional Semiconducting Boron Carbides. *Nanoscale* 11, 11099 (2019).
63. Sara Reynaud A., Fabrication and characterization of carbon and boron carbide nanostructured materials by dissertation submitted to the graduate school-New brunswick Rutgers. The State University of New Jersey in partial Fulfillment of the Requirements. (2010).
64. F. Thévenot, Boron Carbide-a Comprehensive Review. *J. Eur. Ceram. Soc.* 6, 205 (1990).

65. D.D. Radev, and Z. Zakhariev, Structural and Mechanical Properties of Activated Sintered Boron Carbide-based Materials. *J. Solid State Chem.* 137, 1 (1998).
66. M.S. Mahabal, M.D. Deshpande, T. Hussain, and R. Ahuja, Sensing Characteristics of a Graphene-Like Boron Carbide Monolayer Towards Selected Toxic Gases. *Chem. Phys. Chem.* 16, 3511 (2015).
67. S. M. Aghaei, M. M. Monshi, I. Torres, and I. Calizo. *Adsorption and Dissociation of Toxic Gas Molecules on Graphene-like BC3: A Search for Highly Sensitive Molecular Sensors and Catalysts*, ArXiv 1 (2017).
68. S. Mehdi Aghaei, M.M. Monshi, I. Torres, S.M.J. Zeidi, and I. Calizo, DFT Study of Adsorption Behavior of NO, CO, $NO_2$, and $NH_3$ Molecules on Graphene-like $BC_3$: a Search for Highly Sensitive Molecular Sensor. *Appl Surf Sci* 427, 326 (2018).
69. S.R. Naqvi, T. Hussain, S.R. Gollu, W. Luo, and R. Ahuja, Superior Sensitivity of Metal Functionalized boron Carbide ($BC_3$) Monolayer Towards Carbonaceous Pollutants. *Appl. Surf. Sci.* 512, 145637 (2020).
70. Z. Zhao, Y. Yong, R. Gao, S. Hu, Q. Zhou, X. Su, Y. Kuang, and X. Li, Adsorption, Sensing and Optical Properties of Molecules on $BC_3$ Monolayer: First-principles Calculations. *Mater. Sci. Eng. B Solid-State Mater. Adv. Technol.* 271, 115266 (2021).
71. Aref Aasi, Sadegh Mehdi Aghaei, and Balaji Panchapakesan, Outstanding Performance of Transition-metal-decorated Single-layer Graphene-like $BC_6N$ Nanosheets for Disease Biomarker Detection in Human Breath. *ACS Omega* 6, 4696–4707 (2021). https://doi.org/10.1021/acsomega.0c05495.
72. M.C. Malin et al., *Planar Hexacoord. Carbon* 290, 1937 (2000).
73. S. Ahmed, A. Jalil, S.Z. Ilyas, A. Hassan, A. Ilahi, I. Ahmed, M. Khan, and Q. Khan, Ab-Initio Characterization of $B_4C_3$ Monolayer as a Toxic Gases Sensing Material. *Appl. Surf. Sci.* 544, 148877 (2021).
74. H. Chang, K. Tu, X. Zhang, J. Zhao, X. Zhou, and H. Zhang, $B_4C_3$ Monolayer with Impressive Electronic, Optical, and Mechanical Properties: a Potential Metal-free Photocatalyst for $CO_2$ Reduction Under Visible Light. *J. Phys. Chem. C* 123, 25091 (2019).
75. D. Joubert, From Ultrasoft Pseudopotentials to the Projector Augmented-wave Method. *Phys. Rev. B - Condens Matter. Mater Phys.* 59, 1758 (1999).
76. J.P. Perdew, K. Burke, and M. Ernzerhof, Generalized Gradient Approximation Made Simple. *Phys. Rev. Lett.* 77, 3865 (1996).
77. J.P. Perdew, K. Burke, and M. Ernzerhof, Perdew, Burke, and Ernzerhof Reply. *Phys. Rev. Lett.* 80, 891 (1998).
78. S. Grimme, J. Antony, S. Ehrlich, and H. Krieg, A Consistent and Accurate Ab Initio Parametrization of Density Functional Dispersion Correction (DFT-D) for the 94 Elements H-Pu. *J. Chem. Phys.* 132, 154104 (2010).
79. J. Heyd, G.E. Scuseria, and M. Ernzerhof, Hybrid Functionals Based on a Screened Coulomb Potential. *J. Chem. Phys.* 118, 8207 (2003).
80. D. Farmanzadeh, and S. Ghazanfary, The Effect of Electric Field on the Interaction of Glycine with (6, 0) Single-walled Boron Nitride Nanotubes. *J. Serbian Chem. Soc.* 78, 75 (2013).
81. G. Henkelman, A. Arnaldsson, and H. Jónsson, A Fast and Robust Algorithm for bader Decomposition of Charge Density. *Comput. Mater. Sci.* 36, 354 (2006).
82. Z. Cui, X. Wang, Y. Ding, E. Li, K. Bai, J. Zheng, and T. Liu, Adsorption of CO, $NH_3$, NO, and $NO_2$ on Pristine and Defective g-GaN: Improved Gas Sensing and Functionalization. *Appl. Surf. Sci.* 530, 147275 (2020).
83. X. Liu, Y. Chen, M. Zhang, and C. Zhang, Adsorption Properties of Formaldehyde on $B_{12}$-Borophene Surfaces: a First-Principles Study. *Chem. Phys. Lett.* 739, 137035 (2020).
84. P. Ou, P. Song, X. Liu, and J. Song, Superior Sensing Properties of Black Phosphorus as Gas Sensors: a Case Study on the Volatile Organic Compounds. *Adv. Theory Simulat.* 2, 1 (2019).
85. J.S. Kim, H.W. Yoo, H.O. Choi, and H.T. Jung, Tunable Volatile Organic Compounds Sensor by Using Thiolated Ligand Conjugation on $MoS_2$. *Nano Lett.* 14, 5941 (2014).
86. W. Ai, L. Kou, X. Hu, Y. Wang, A.V. Krasheninnikov, L. Sun, and X. Shen, Enhanced Sensitivity of $MoSe_2$ Monolayer for Gas Adsorption Induced by Electric Field. *J. Phys. Condens. Matter* 31, 445301 (2019).
87. Q. Zhou, L. Yuan, X. Yang, Z. Fu, Y. Tang, C. Wang, and H. Zhang, DFT Study of Formaldehyde Adsorption on Vacancy Defected Graphene Doped with B, N, and S. *Chem. Phys.* 440, 80 (2014).
88. A. Shokuhi Rad, and V. Pouralijan Foukolaei, Density Functional Study of Al-Doped Graphene Nanostructure Towards Adsorption of CO, $CO_2$ and $H_2O$. *Synth. Met.* 210, 171 (2015).
89. Y. Su, Z. Ao, Y. Ji, G. Li, and T. An, Adsorption Mechanisms of Different Volatile Organic Compounds onto Pristine $C_2N$ and Al-Doped $C_2N$ Monolayer: A DFT Investigation. *Appl. Surf. Sci.* 450, 484 (2018).
90. Z. Wu, J. Zhou, D. Li, Z. Ao, T. An, and G. Wang, Density Functional Theory Study on the Enhanced Adsorption Mechanism of Gaseous Pollutants on Al-Doped $Ti_2CO_2$ Monolayer. *Sustain. Mater. Technol.* 29, e00294 (2021).
91. R. Chandiramouli, Structural and Electronic Properties of Germanane Nanosheet Upon Molecular Adsorption of Alcohol and Aldehyde Molecules: DFT Comparative Analysis. *J. Mol. Liq.* 242, 571 (2017).
92. V. Nagarajan, and R. Chandiramouli, Interaction of Alcohols on Monolayer Stanane Nanosheet: a First-principles Investigation. *Appl. Surf. Sci.* 419, 9 (2017).
93. W. Guo, S.G. Surya, V. Babar, F. Ming, S. Sharma, H.N. Alshareef, U. Schwingenschlögl, and K.N. Salama, Selective Toluene Detection with $Mo_2CT_xMXene$ at Room Temperature. *ACS Appl. Mater. Interf.* 12, 57218 (2020).
94. R. Majidi, and A.R. Karami, Adsorption of Formaldehyde on Graphene and Graphyne. *Phys. E Low-Dimens. Syst. Nanost.* 59, 169 (2014).
95. M. Chi, and Y.P. Zhao, Adsorption of Formaldehyde Molecule on the Intrinsic and Al-Doped Graphene: a first Principle Study. *Comput. Mater. Sci.* 46, 1085 (2009).
96. M. Moradi, M. Noei, and A.A. Peyghan, DFT Studies of Si- and Al-doping Effects on the Acetone Sensing Properties of BC3 Graphene. *Mol. Phys.* 111, 3320 (2013).
97. S. Agrawal, G. Kaushal, and A. Srivastava, Electron Transport in C3N Monolayer: DFT Analysis of Volatile Organic Compound Sensing. *Chem. Phys. Lett.* 762, 138121 (2021).
98. H. Guo, K. Zheng, H. Cui, J. Yu, L.Q. Tao, X. Li, C. Liao, L. Xie, and X. Chen, Tellurene Based Biosensor for Detecting DNA/RNA Nucleobases and Amino Acids: a Theoretical Insight. *Appl. Surf. Sci.* 532, 147451 (2020).
99. W. C, O. C, S. B. on 2D M. Tan and K. W. Ang, *V,* Adv. Electron. Mater. **7**, 1 (2021).
100. A. Vaidyanathan, M. Mathew, S. Radhakrishnan, C.S. Rout, and B. Chakraborty, Theoretical Insight on the Biosensing Applications of 2D Materials. *J. Phys. Chem. B* 124, 11098 (2020).
101. Y.Y. Broza, and H. Haick, Nanomaterial-based Sensors for Detection of Disease by Volatile Organic Compounds. *Nanomedicine* 8, 785 (2013).
102. W.Y. Chen, S.N. Lai, C.C. Yen, X. Jiang, D. Peroulis, and L.A. Stanciu, Surface Functionalization of $Ti_3C_2T_xMXene$ with Highly Reliable Superhydrophobic Protection for Volatile Organic Compounds Sensing. *ACS Nano* 14, 11490 (2020).

103. Q. Wan, Y. Xu, and H. Xiao, Exhaled Gas Detection by Ir-Doped CNT for Primary Diagnosis of Lung Cancer. *AIP Adv.* 8, 105128 (2018).
104. T. Liu, Z. Cui, X. Li, H. Cui, and Y. Liu, Al-Doped Mose2 Monolayer as a Promising Biosensor for Exhaled Breath Analysis: a DFT Study. *ACS Omega* 6, 988 (2021).
105. T. Hussain, P. Panigrahi, and R. Ahuja, Enriching Physisorption of $H_2S$ and $NH_3$ Gases on a Graphane Sheet by Doping with Li Adatoms. *Phys. Chem. Chem. Phys.* 16, 8100 (2014).
106. H. Cui, P. Jia, X. Peng, and P. Li, Adsorption and Sensing of CO and $C_2H_2$ by S-Defected $SnS_2$ Monolayer for DGA in Transformer Oil: A DFT Study. *Mater. Chem. Phys.* 249, 123006 (2020).